FINAL REPORT: MODELING MINKE WHALE HEARING

SUBMITTED TO: JOINT INDUSTRY PROGRAM

Submitted by:

Darlene R. Ketten, Ph. D. (Principal Investigator, Technical Contact)
Senior Scientist
Biology Department
Woods Hole Oceanographic Institution
MS#50, Marine Resources Facility
Woods Hole, Mass. 02543

Asst. Clinical Professor
Department of Otology and Laryngology
Harvard Medical School
Office: 508 289 2731 (WHOI) FAX: 508 457 2028
dketten@whoi.edu
http://csi.whoi.edu

David Mountain, Ph. D. (Co-Principal Investigator)
Professor
Biomedical Engineering
Boston University
44 Cummington St.
Boston, MA 02215
Office: (617) 353-4343 FAX: (617) 353-6766
dcm@bu.edu

Keywords: Marine mammal, baleen whale, minke whale, seismic, sonar, hearing range, hearing sensitivity, auditory system, power flow model

PROJECT SUMMARY

The primary goal of this research was to provide a proof of concept for employing modeling techniques to provide reliable hearing estimates for species thought to be most liable to impacts from common, active sound sources deployed in the oceans, including seismic operations. These data are necessary for determining ranges of interest for playback experiments and for species specific risk assessments for hearing impacts. The anatomical investigations, because they involve whole head analyses, may also assist in determining effective electrode and sound source placements for future efforts on auditory brainstem response (ABR) measures in live stranded baleen whales.

To address the primary question, the progressive goals in this project were to acquire sufficient specimens of minke whale heads and ears, to document the anatomy via CT, dissection, and histology, to obtain middle and inner ear morphometrics, and to obtain middle and inner ear stiffness measures. From these data, both anatomical amd experimental, two forms of model audiograms of minke whale hearing were formulated. using current anatomical and biomedical engineering techniques. . Hearing range models were produced by both methods for the minke whale and for two odontocetes, the bottlenose dolphin and the harbor porpoise. The purpose of the odontocete analyses were to test the validity of the models by comparing model data with previously published live animal psychophysical audiograms.

The required data in all categories was completed. Anatomical measures were obtained for both entire heads and for middle and inner ears. The anatomical team (Ketten/WHOI) completed a frequency range map for the minke based on basilar membrane dimensions and cochlear canal morphometry obtained via CT and histologic measurements. Models from anatomical measurements of inner ear structures are based on thickness and width measurements which correlate with basilar membrane resonances that determine the hearing range and frequency resolution of mammalian inner ears. The advantage of this technique is that it provides a rapid estimate of entire hearing range and can be used on inner ears from a wide range of post mortem conditions in any species. These investigations also found evidence of peribullar fatty tissues that may be functional analogues to the “acoustic fats” reported to play a key role in odontocete sound reception.

Ear specimens provided to the BU team were used for point stiffness measure of the membrane and ossicular motion using a piezo electric system specifically designed to accommodate larger minke specimens.Models based on direct point displacement measures of middle and inner ear components estimate stiffness for modeling middle ear responses, transfer functions, and basilar membrane positional stiffness. The advantage of this technique is that it gives accurate estimates of peak frequencies for the middle ear responses and greater precision measures of inner ear stiffness from fresh ears.

PROJECT OVERVIEW

The research effort involved two integrated teams:

> An **Anatomical Analysis Team** (WHOI) led by Darlene Ketten that characterized head, middle, and inner ear structures of the candidate species. Personnel working on this team included **Dr. Ketten (PI), Scott Cramer (website and archive manager), Julie Arruda (CT technologist), and Maya Yamato (graduate student).**
>
> A **Physiological Modeling Team** (BU) led by David Mountain that implemented auditory response models using the anatomical data and develop the species-specific model audiogram. Personnel working on this team included **Dr. Mountain (PI), Aleks Zosuls (engineer), and Andrew Tubelli (graduate student).**

This project has three major aims divided between the two teams as follows:

I. Development of a morphometric database for minke whale heads and inner ears (WHOI);

II. Direct stiffness measures of the middle ear and of representative points of the inner ear membrane (BU);

III. Completion, testing, and publication of a model, generic minke whale audiogram (WHOI/BU).

AIM I (WHOI):

Anatomical Substrates of Hearing

This aim consists of developing a biomedical scan and histology derived database of minke whale ear anatomy for model development

AIM I:
SUMMARY OF ACCOMPLISHMENTS (SEE ALSO PUBLICATIONS)

The Anatomical Analysis Team (AIM I/WHOI) had as its goal to characterize head, middle, and inner ear structures of the candidate species.

Minke whale heads and ears were scanned at 0.1 mm increments, reconstructed, and segmented for soft and bony tissue elements. Whole heads were segmented for bone, airways, and muscle and organs groups. Ears were segmented for fat, bone, neural, and fluid labyrinth elements in order to demonstrate the cochlear turn distribution, radii ratios, and axial heights. A significant finding in the whole head scans is the presence of fatty tissues adjacent to the middle ear cavity which may function in the same way as specialized fats in the odontocetes; i.e., as an outer ear analogue.

Three-dimensional reconstructions of the intact ears, middle ear ossicles, and inner ear as well as 5 whole specimens with morphometric data were transferred to the BU team for further analyses.

The histologic sections have also yielded the first data on longitudinal variations in basilar membrane dimensions for this species. The data show the inner ear to be consistent with a 9-10 octave hearing range that is primarily adapted for mid to lower frequencies and with cochlear ratios consistent with better resolution and propagation to the apical, low frequency encoding region of the inner ear than is seen in odontocete ears.

Methods

Examples of the research case files, representative scans, reconstructions, and information on the related facilities and procedures can be viewed at the Ketten Laboratory website: **http://csi.whoi.edu**

Whole animals, whole heads, and extracted ears were processed in a step-wise manner comprising external assessment, CT and/or MRI examination, gross dissection, and, for selected specimens, processing for celloidin histology. CT Examinations were obtained at the WHOI CSI facility on a Siemens Volume Zoom with the following protocols: 0.5 mm acquisitions. 1024 matrix raw data archived, 512 matrix images archived, primary images in transaxial plane, bone and soft tissue window formats, with both conventional and extended (42,500 HU) scales. Effective mA and kV were varied according to tissue masses.

Gross dissections were conducted at the WHOI MRF facility. Celloidin histologies were obtained following the conventional decalcification procedures for mammalian ears (Ketten, 1992) and were completed using the facilities of the Temporal Bone Bank, Massachusetts Eye and Ear Infirmary, Harvard Medical School. Ears were decalcified in EDTA, dehydrated in graded alcohol series, embedded in celloidin, sectioned at 30 microns, stained with hematoxylin and eosin, and mounted on glass slides for examination.

Morphometric data were obtained from the 2D images and tissue sections and as described and illustrated below also from 3D visualizations that afforded consistent modiolar and radial sectioning views across specimens. 3D reconstructions were obtained using Siemens VRT and Shaded Display proprietary software as well as Amira and Osirix programs on 32-bit and 64 bit PC and Apple Platforms

Specifics of each of these study areas are as follows.

Task 1: Milestones

1.1 Complete CT of survey of intact ear complexes and gross description and measurements of ears

Under the JIP funding, a total of 15 scan sets and 9 complete scan, histology, and measurement series were completed. These comprised 10 CT odontocete cases employed as controls (*Tursiops* and *Phocoena*) from which 7 histology cases were examined (200-500 sections each). For the minke whales, 5 CT scan sets of intact minke whale heads were completed from which 7 ears were harvested fresh (Figure 1). Of these 2 full histologies were completed (1200 sections each). Details of minke specimens collected under JIP funding and their examination and dispositions are included in Appendix I at the end of this report. In addition, 14 ears from 7 other animals and five brains with the auditory centers intact were scanned and preserved for possible future analyses. Two intact ears and surrounding associated peribullar and fatty tissues were also been examined with MRI. These head and ear scans provided the first multi-individual, comprehensive, matrix-based, species-specific databases of head and ear anatomy and tissue density maps of a baleen species head with undisturbed internal anatomy. These scans are being employed in an on-going FEM analysis project under funding by other agencies.

Figure 1A. Juvenile minke whale head prepared for Computerized Tomographic (CT) imaging.

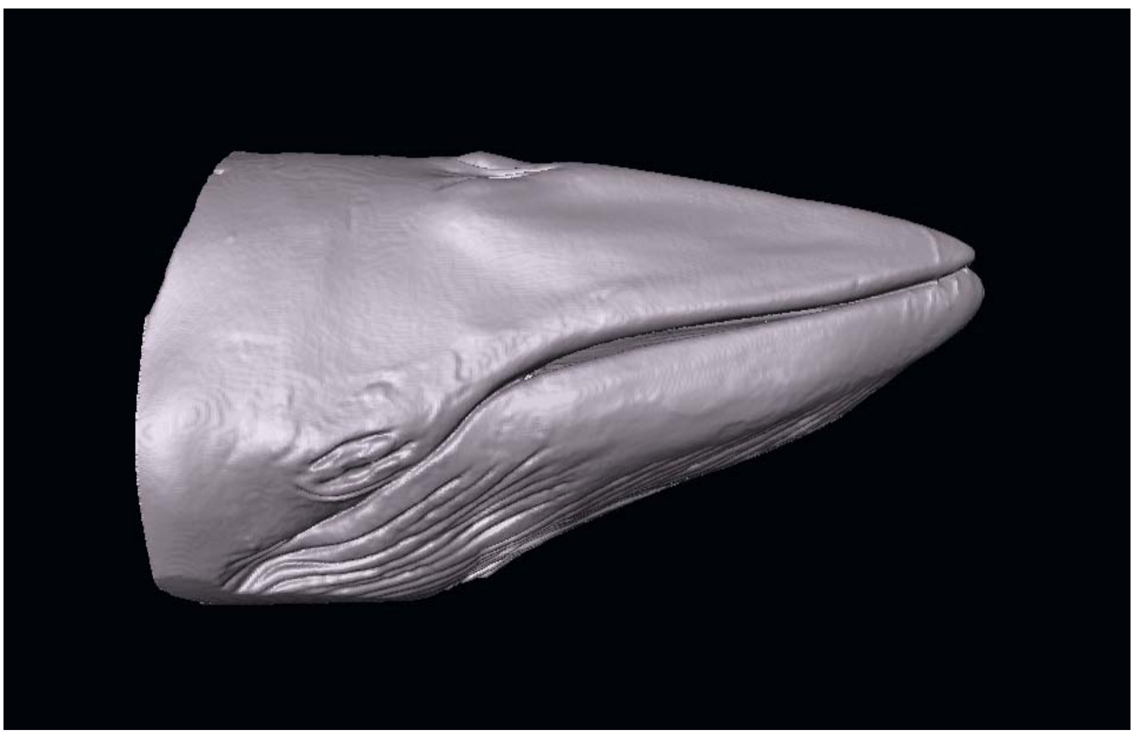

Figure 1B. 3D Surface Rendering using AMIRA® visualization software from 3 mm CT scans of the head of juvenile minke whale (*Balaenoptera acutorostrata*) shown prior to scanning in Fig. 1A.

From these tissues and techniques, mandibular fat bodies have been identified proximal to and in communication with the middle ear (Fig.2). These tissues are consistent in shape and volume across individuals and are similar in consistency and color to fats that are known to be an essential component of toothed whale auditory systems (Ketten, 1992; Ketten, 2000, Koopman et al 2006). Samples of these fats were sent to Dr. Heather Koopman (UNC Wilmington) for biochemical analyses.

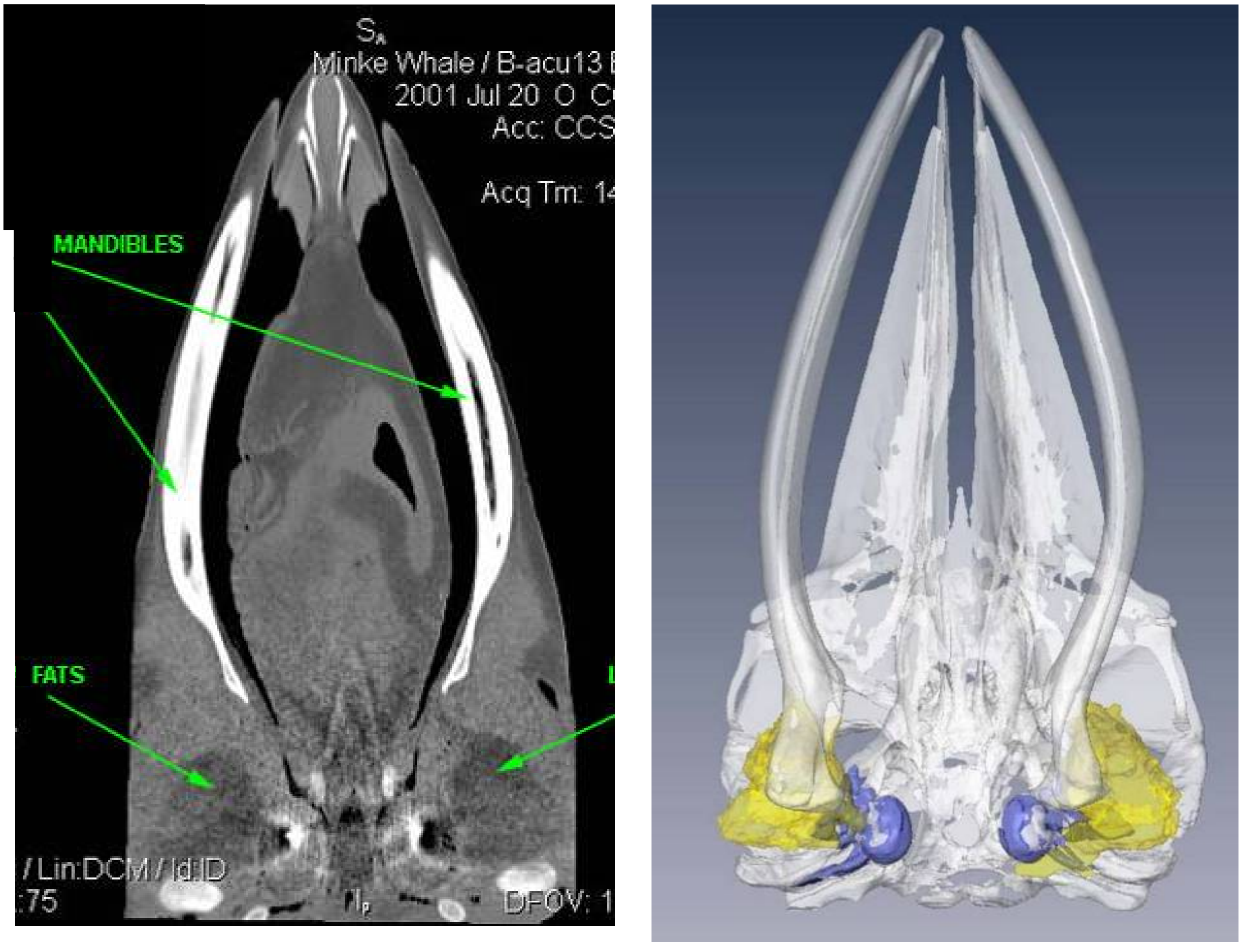

Figure 2A. Left image shows a 2D CT section image reformatted in the coronal plane of a minke whale head obtained on the WHOI Siemens Volume Zoom CT scanner. The right image is a VRT rendering from this case using Siemens software to demonstrate the relationship and shape of the skull elements (white), peribullar fats (yellow), and ears (blue). The head is 56 cm in diameter and 120 cm in length.

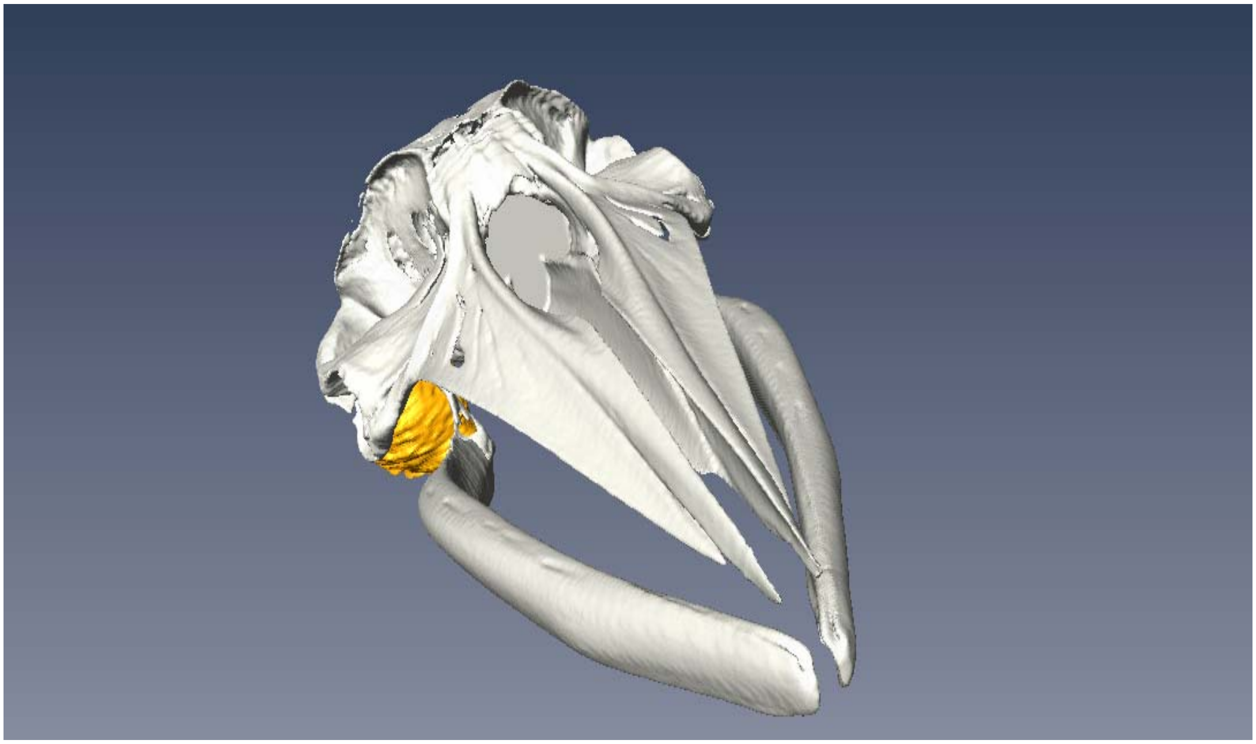

Figure 2B. 3D VRT Rendering from 3 mm CT scans of a juvenile minke whale (*Balaenoptera acutorostrata*) using AMIRA® software to segment and visualize bone and peribullar fats (yellow).

1.2 Identify practice specimens and distribute to BU

Five ears were documented and transported to BU for the purpose of point stiffness measurement (see BU team report for details of measurements)..

Middle Ear Anatomy

Three-dimensional reconstructions from the transaxial section data were used to measure the middle ear cavity and ossicular dimensions at consistent orientations and for determining *in situ* angles of the ossicular chain. In some cases, volumes were obtained for comparison from 3D reconstructions with calculations by Amira and Siemens software. The dissections also demonstrated that the fatty body contacts the wax plug and "glove finger" which is the highly derived, fibrous, elongated tympanic membrane that is unique to mysticetes (Fig. 3)

1.3 Complete measures of middle ear morphometry from CT

Volume tests using known volumes of water in Erlenrmeyer flasks were unsatisfactory for the first Amira software version available in the first half of this project. Siemens software volumes were within 3% of known volumes with estimates optimized if 0.1 mm sections were used, however, the Siemens software does not provide morphometry for 3D renderings. Errors in the Amira program were corrected by the company in the version 5. Tests of this software using calibrated fluid volumes show an error of less than 2%, consistent with the Siemens values. The minke has an average middle ear volume of 158.3 cm^3 (n = 3: 157.0, 158.0, 160.0 cm^3) which is consistent with that of elephants and other LF specialists (Fig. 3)

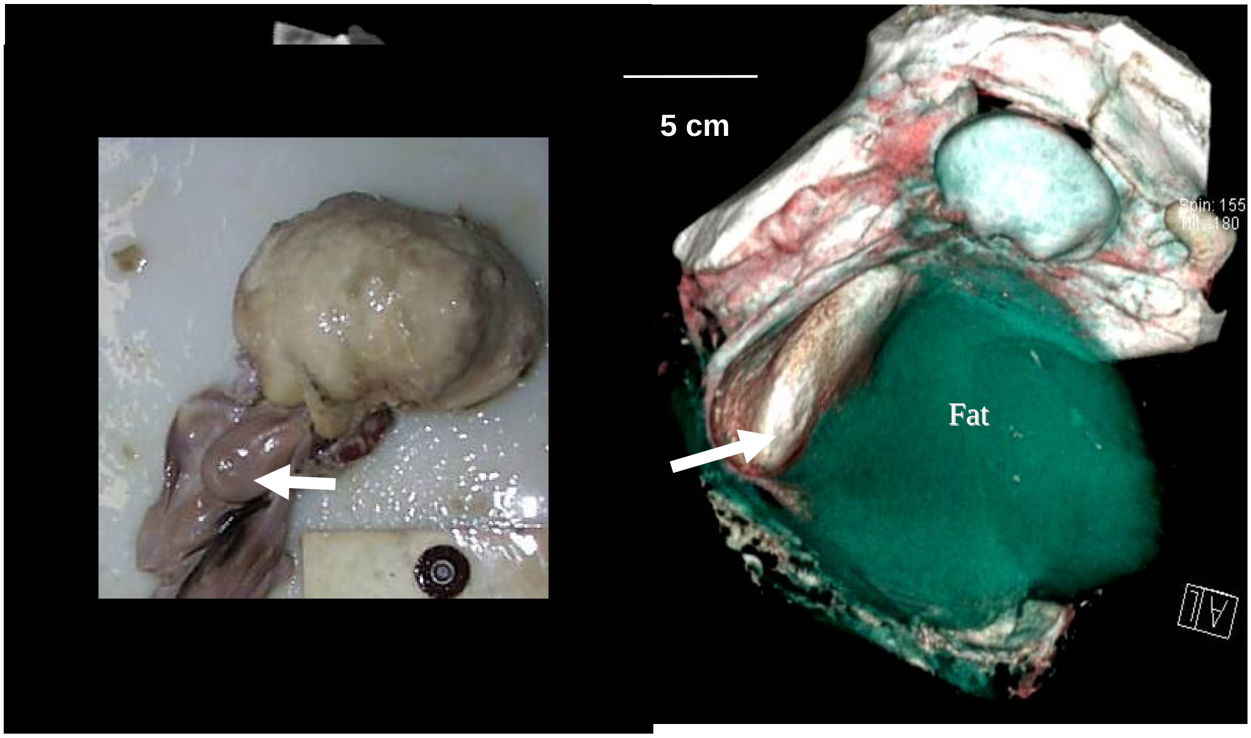

Figure 3. The left image shows an extracted, dissected left ear of a minke whale in lateral view. The arrow points to the glove finger. The bulbous bone at the top of the photo is the tympanic bulla, which forms the middle ear cavity. The right image is a 3D CT multi-segmentaion of a minke demonstrating the relationship of the fatty tissues (green) with the glove finger (arrow) and the tympanic bulla.

Task 2: Cochlear Anatomy and Morphometry

The objective of this task was to obtain quantitative, topographic maps of cochlear cytoarchitecture for each ear. Measurements and descriptions of minke whale auditory anatomy are based on 3-D reconstructions of 0.1 mm CT scan sections and registered light microscope sections.

Micro CT images of ears from other mammals that are required for controls of the model data were transferred from Boston University to WHOI for analysis and image reconstruction. Comparison of image resolution was made between standard and micro CT images of the same species to determine the most useful scanning technique in assessing auditory function. A new technique was also devised for employing CT data as a guide for locating the basilar membrane within the uncut periotic bone.

Milestones

Accomplished:

2.1 Complete micro CT and micro MRI of inner ears
Accomplished:

Micro CT has been accomplished on two control species ears. Micro MRI was completed on one specimen. The images obtained to date for minke whales are unsatisfactory due to ring and stellate artifacts which results from too low an accelerating voltage for penetration of the tissue and detector failures in the machine. A second machine was identified for use at AFIP in Washington, DC, and collaborative access was arranged, but there were insufficient funds for completing this option. The best images obtained to date remain the 0.1 mm sections obtained at the WHOI facilities (Fig. 4).

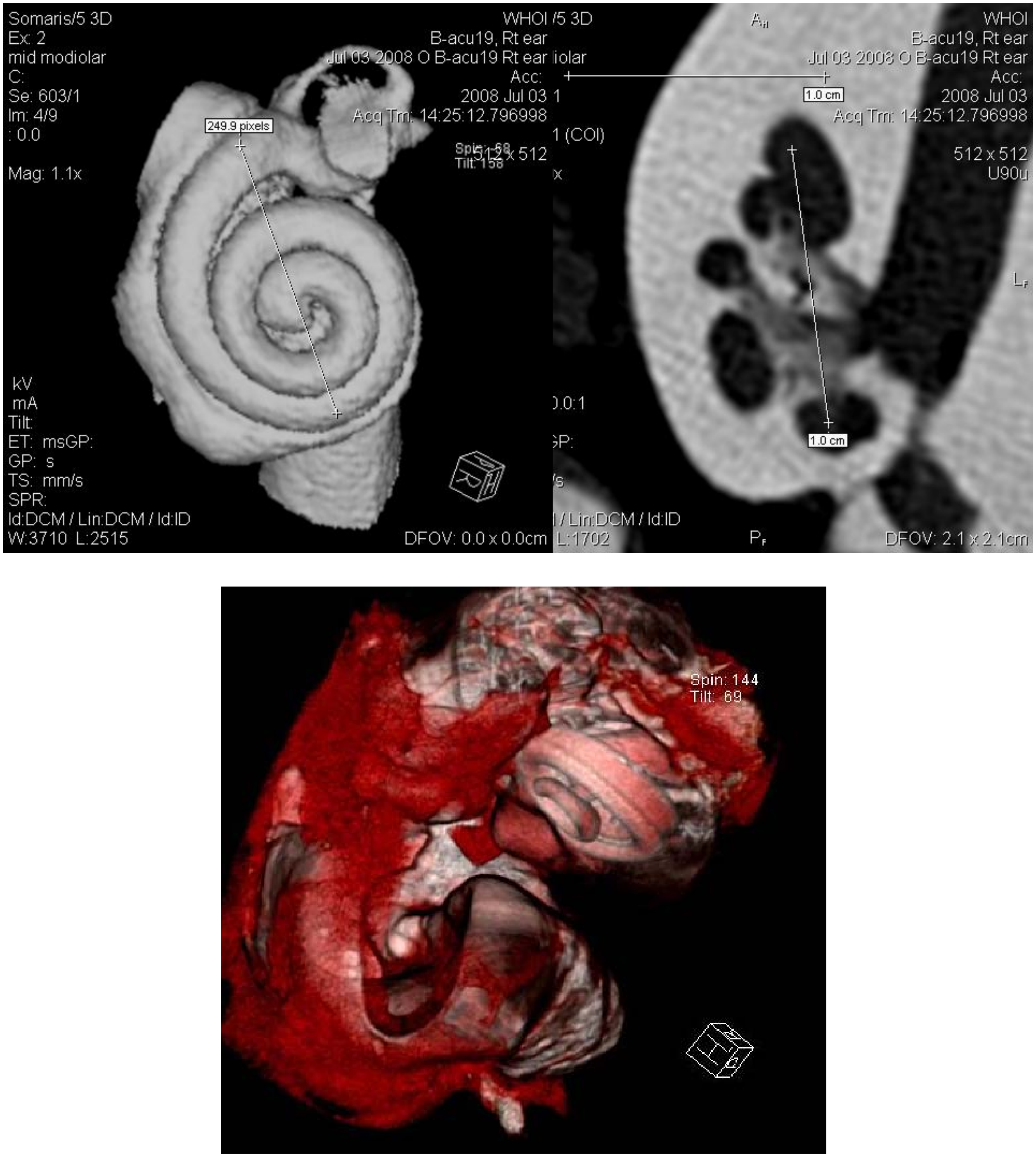

Figure 4. The upper left image shows shaded surface visualization of the inner ear labyrinth of a minke whale. The upper right image is a 0.1 mm paramodiolar image of the cochlea. The lower image shows a VRT rendering of the entire ear with the periotic bullar surface removed to reveal the cochlear spiral. The cochlea is 10 mm in diameter. The arrow points to the ossicular chain.

2.2 Complete additional section staining and digitizations

Two minke ears have been processed through decalcification, embedding in celloidin, sectioning, staining, and mounting. Additional ears began processing but their completion is not funded through this project.

2.3 Complete basilar membrane and neural measurements from histology

Measurements from one ear are completed. A second ear was processed through decalcificaton and is ready for analysis pending additional funding from an alternative source. Data from the completed ear are shown in figures 5 and 6.

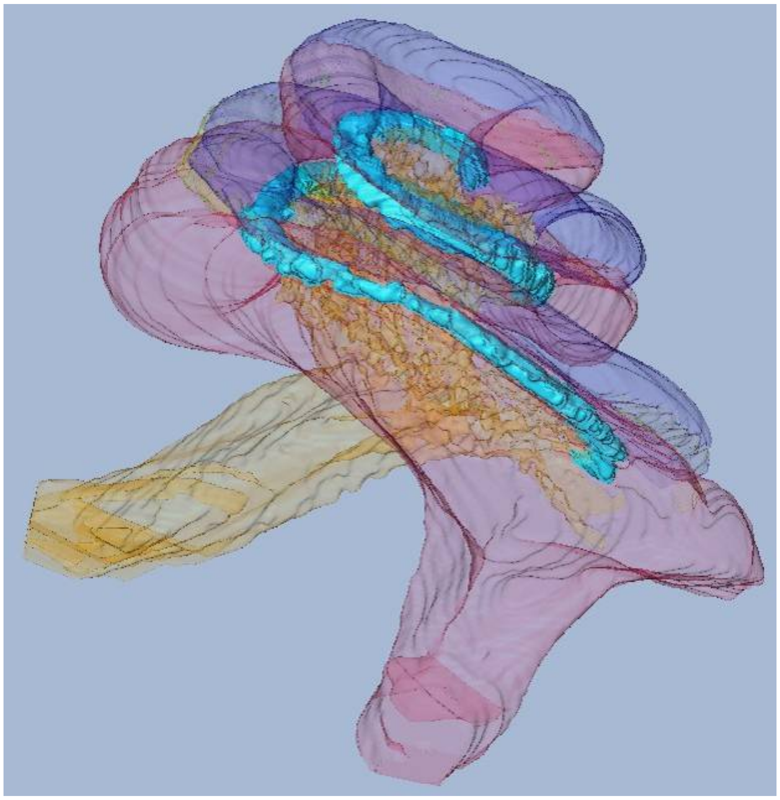

Figure 5. The image shows a 3D visualization of the cochlear scalae (pink and blue), the VIIIth nerve (gold) and the basilar membrane (blue) of a minke whale.

Hearing ranges and frequency estimates can be made for mammalian inner ears based on the thickness and width dimensions of the basilar membrance (Ketten, 1994, 2000).I nitial measurements for the minke membranes were obtained from histologies, however, because these represent true cross-sections only in the mid-modiolar region, to obtain more accurate measures, they were reconstructed and then sub-sectioned radially (Fig. 6). Estimates of frequencies were obtained using the formulations and methodologies described in Ketten et al (1998) and are shown in Table 1. Absent data points are due to a lack of membrane as a result of post mortem loss of the membrane in the ear examined. For the two ears for which measures were completed to date from CT and/or histology, the dimensions are as follows:

Basal diameter: 12.5, 12.3

Axial height: 7.25, 7.5,

Length: 44.36, 44.76 mm

Basal width: 0.13 mm

Basal Thickness: 0.005 mm

Apical width: 0.51 mm (1.2 mm)

Apical Thickness: 0.003 (0.002)

Turns: 2.25

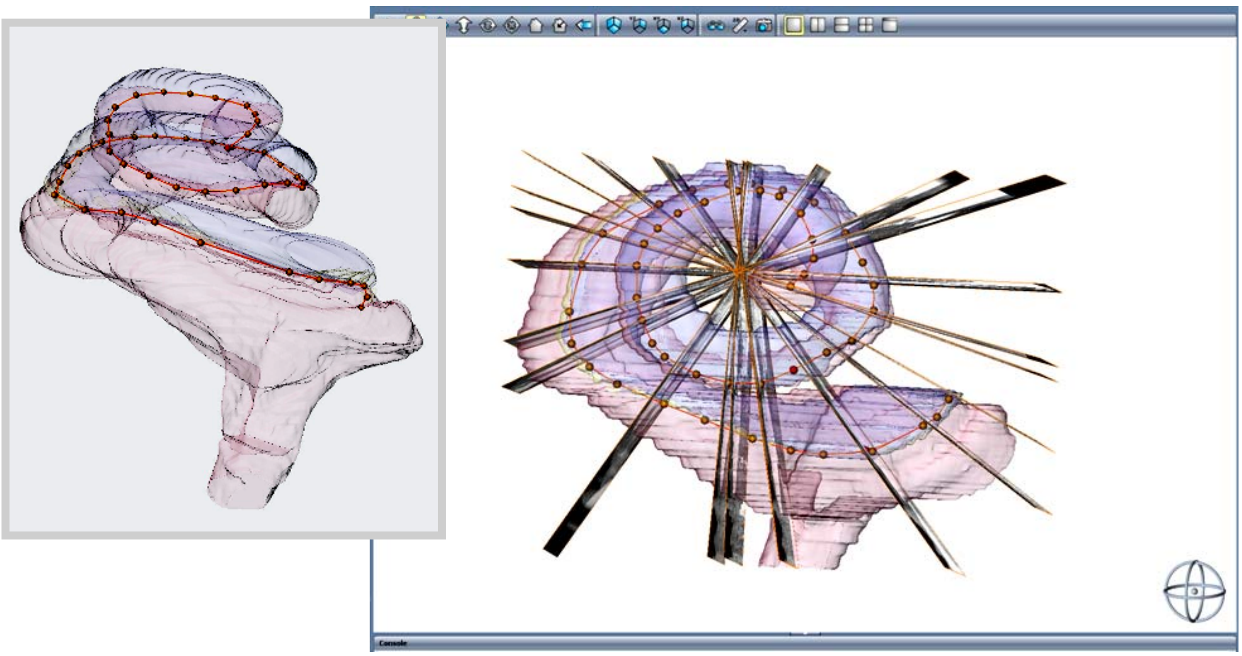

Figure 6. The red line with spheres along spiral indicate the position of the basilar membrane.

Calculations of frequency from the anatomy indicate an average functional frequency range of 17 Hz to 35 kHz. As with other species, the functional range does not include frequencies that may be encoded in the sparsely innervated basal-most and apical-most 5% of cochlear lengths. These data are shown graphically in figure 7 and 8. The estimates are also consistent with the cochlear ratios, which were demonstrated to be a significant feature for LF acuity (Manoussaki et al 2008) as shown in Table 2. These findings are in close agreement with the point stiffness data determined in Project 2 (see below).

Table 1

Minke Whale Frequency Estimates from Histologic Morphometry

% Length from Base	**Width (mm)**	**Thickness (mm)**	**T:W**	**Predicted Frequency (kHz) Base (High) to Apex (Low)**
0	-	-	-	
6	0.130	0.0110	0.084615	25.90
10	0.170	0.0083	0.048824	11.99
15	-	-	-	-
20	-	0.0077	-	-
25	-	0.0068	-	-
30	0.200	0.0064	0.032000	10.25
35	0.270	0.0065	0.024074	6.67
40	0.330	0.0052	0.015758	3.82
45	-	-	-	-
50	-	0.0050	-	-
55	0.460	0.0050	0.010870	0.16
60	0.510	0.0050	0.009804	0.12
80	0.920	0.0030	0.003260	0.020

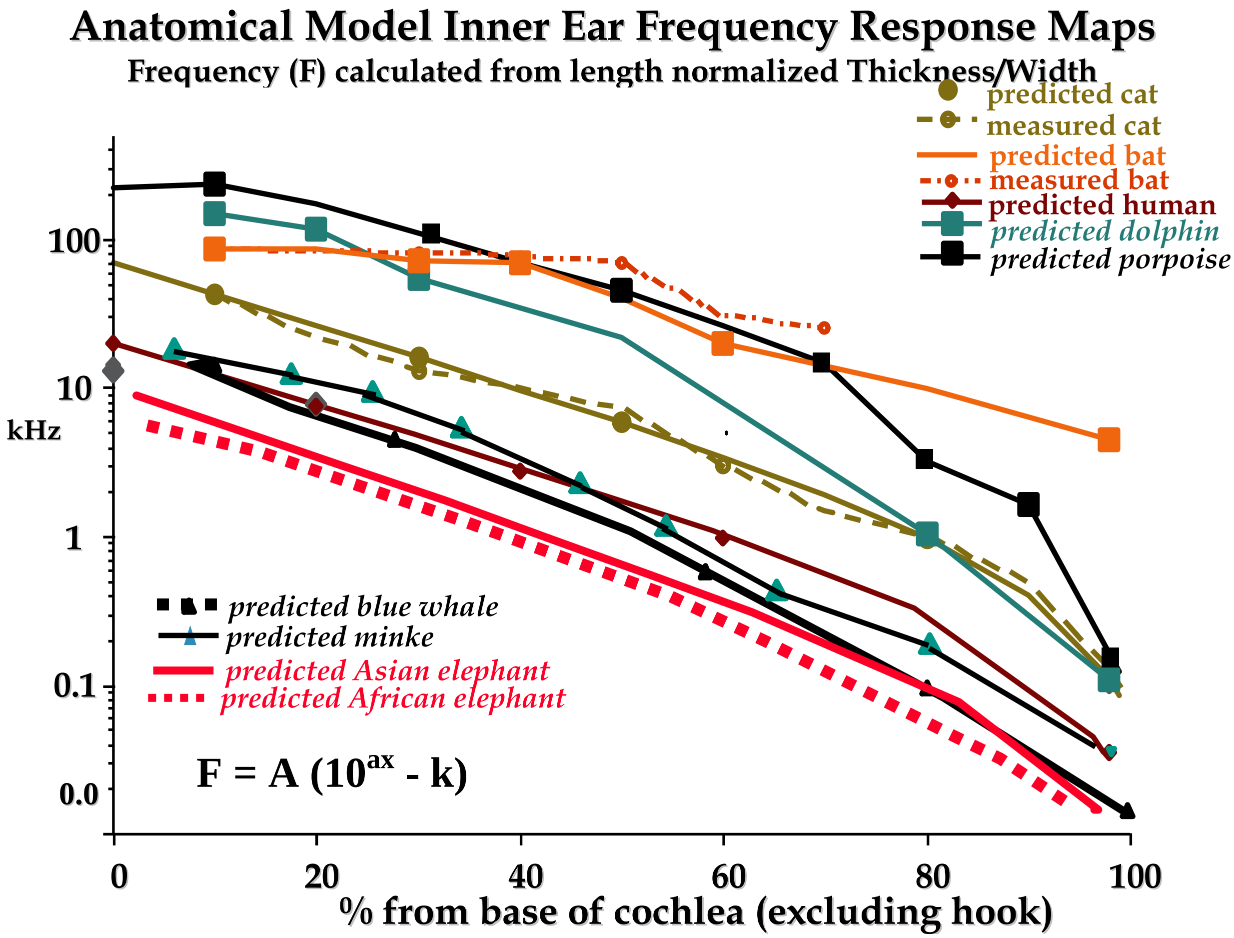

Figure 7. Calculated frequency distributions for representative mammalian cochleae. Because of the radical differences in length amongst species, the cochlear positions are shown as a percentage of length. Measured values obtained via acute electrophysiologic methods for some species were obtained from the literature.

Table 2: Radii Ratios and Low-frequency Limit (see also Manoussaki et al, 2008)

Species	blue whale	right whale	humpback whale	minke whale	bottlenose dolphin	harbor porpoise
Rmax/Rmin	10.7	9.1	7.5	7.0	4.4	3.5
LF Hz	10	12	18	15	150	180

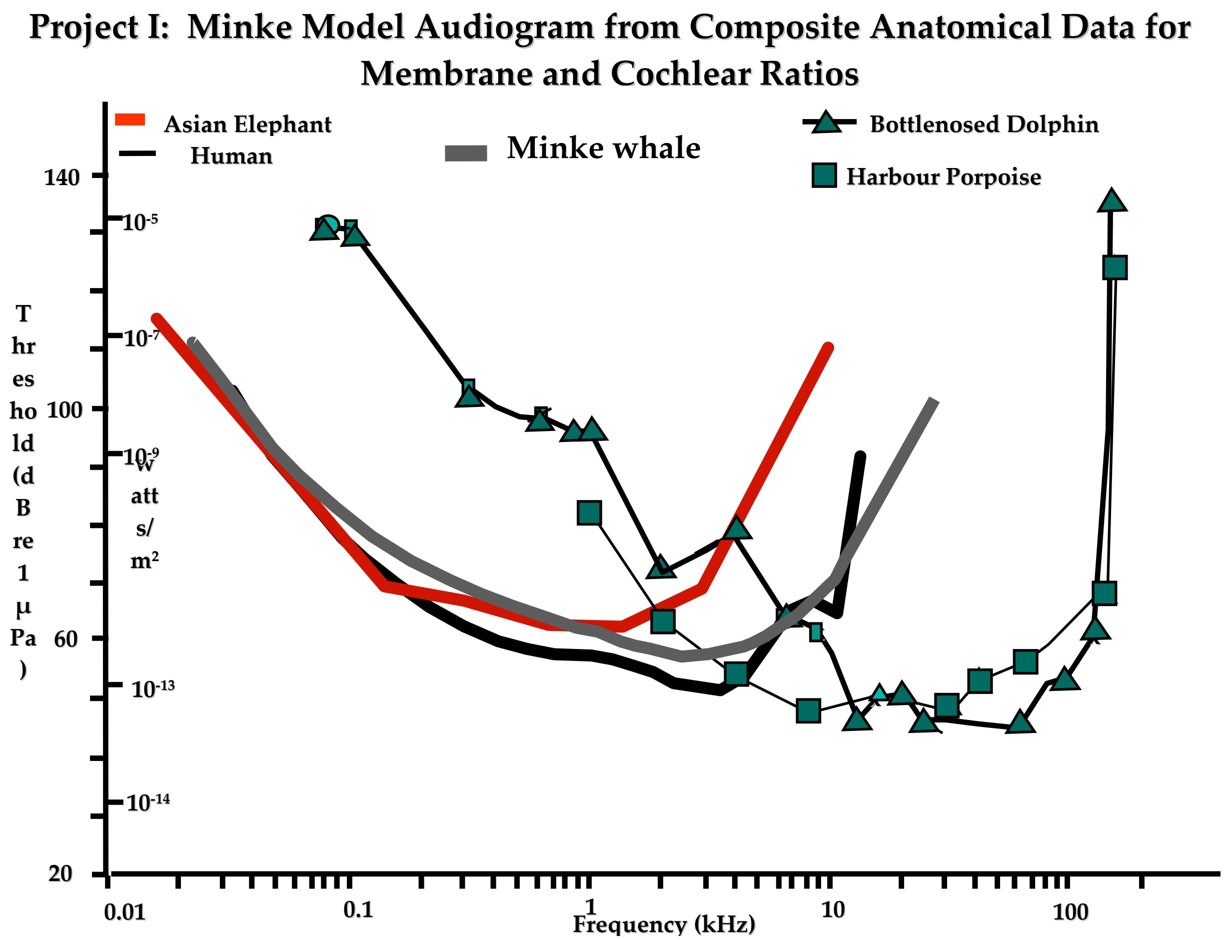

Figure 8. An anatomically derived theoretical audiogram is shown for the minke whale in comparison to behavioural audiograms for other species. The shape of the mink curve and the minimum threshold are speculative at this time.

AIM II (BU):

Project Goals

The primary goal of this project is to develop biophysically based computational models for the hearing capabilities of minke whales. The parameters for these models are derived from anatomical and biomechanical measurements made on ears harvested from stranded animals and the resulting models are used to predict important features such as the audiogram.

Our approach to modeling the auditory periphery is to start with an acoustic power flow model in which the external ear, middle ear, and cochlea are treated as a series of connected acoustical and mechanical systems where outputs from each system provide the inputs for the next (Rosowski, 1994) The mechano-acoustical system comprised of the outer and middle ear (Fig. 1) is modeled as a transformer-coupled pair of two-port networks. The two-port blocks represent the acoustic and mechanical transfer functions of the external ear (H_E) and the middle ear (H_M) respectively. The cochlear block represents the acoustic input impedance, Z_C, of the cochlea The transformer between the external ear and middle ear converts acoustic volume velocity and acoustic pressure U_M and P_M to mechanical velocity V_M and force F_M respectively, while the transformer between the middle ear and cochlea converts the mechanical velocity and force, V_C and F_C, of the ossicular chain back into acoustic velocity and pressure, U_C and P_C respectively. The individual blocks are simulated using finite-difference and finite-element techniques.

It is believed that both inner and middle ear characteristics determine the shape of the mammalian audiogram, but the low and mid-frequency portions of the audiogram are influenced most by the middle ear transfer function (Mountain *et al.*, 2003; Miller *et al.*, 2006). See Rosowski (1994) for an in depth review of the acoustic power flow model. Since most of the sounds associated with oil and gas exploration and production are in the low to mid-frequency region, we have focused most of our efforts on understanding cetacean middle-ear function.

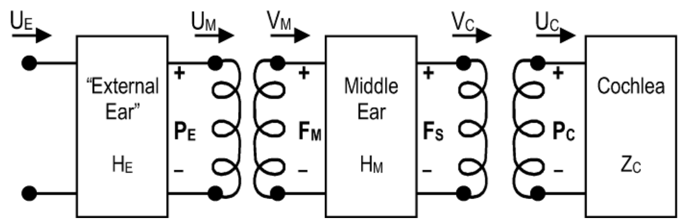

Fig. 1 – Schematic diagram of the acoustic power flow model of hearing. External, middle, and inner ear (cochlea) are each represented as two port networks connected by transformers. Transformers are used to represent the conversion of pressures to forces and volume velocities to particle velocities that occurs between the external, middle, and inner ear.

Accomplishments

The Boston University portion of this project has three primary areas: middle ear measurements, basilar membrane measurements, and simulation studies.

Task 3: Middle Ear Measurements

The geometry and material properties (density, elasticity) of the middle ear bones work together to create a system that couples sound from the external environment to the cochlea. We have reconstructed the geometry using CT scans. Figure 2 illustrates such a reconstruction.

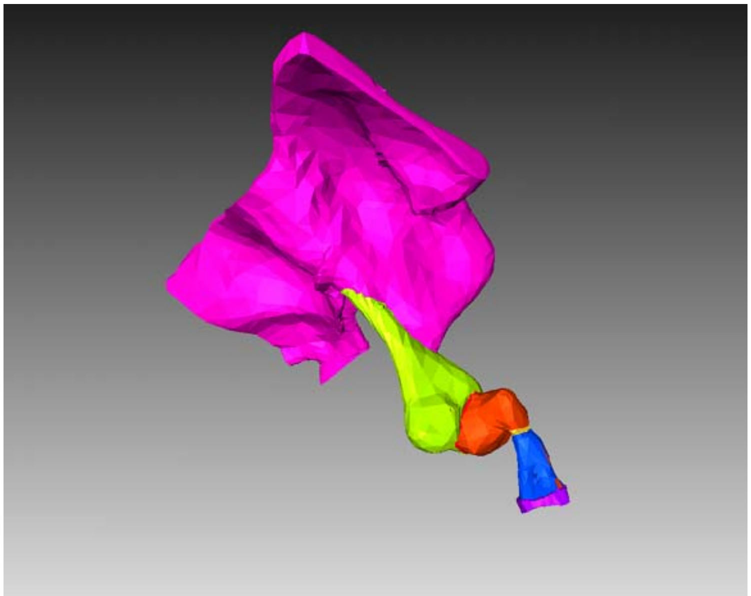

Figure 2. Reconstructed minke middle ear with a portion of the tympanic bone (magenta) The malleus is colored green, the incus red, and the stapes blue.

To measure the elasticity of the ossicular bone, we use nanoindentation. The bone is prepared by cutting sections and then polishing the surface. A nanoindenter system (Hysitron model TI 900 TriboIndenter) was used to measure stress-train curves on slices taken from each of the ossicles. The indenter tip is advanced at a constant rate (20 nm/s) and then retracted at the same rate. Young's modulus was estimated from the retraction phase of the curve using the procedure of Zysset et al. (1999). Figure 3 shows the mean value for minke from our measurements along with values for cat and human. The minke value is somewhat stiffer than the other two species.

Middle ear bone density was estimated by weighing the individual ossicles and then measuring volume using the displaced fluid technique. Generic mammalian values were used for the soft tissue parameters.

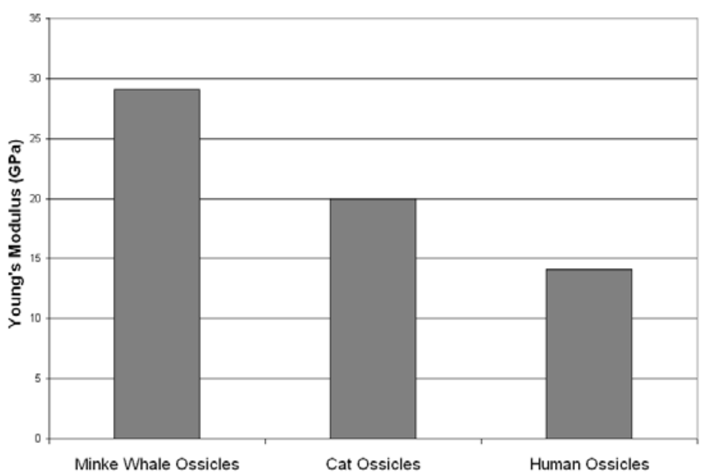

Figure 3. Comparison of Young's modulus for ossicles from three species. The cat value was estimated by Funnell *et al.* (1992) using published data from other labs. The human value is from Prendergast et al. (1999) and Sun *et al.* (2002).

Task 4: Basilar Membrane Measurements

Basilar membrane stiffness was measured using a piezoelectric force probe. The technique used is similar to the system that we developed for use in our previous gerbil studies (Olson and Mountain, 1994; Naidu and Mountain, 1998). The probe tip is positioned under the basilar membrane and displaced sinusoidally by a piezoelectric actuator while force is measured using a piezoelectric sensor. The probe is advanced in 1 µm steps and force measurements are taken at each step. The stiffness (force divided by displacement) is then plotted as a function of probe position (figure 4). The point at which the stiffness-deflection curve exhibits a significant change in slope is used to estimate the physiologically relevant stiffness. This value is used along with the cochlear partition dimensions to estimate the acoustic impedance for modeling purposes.

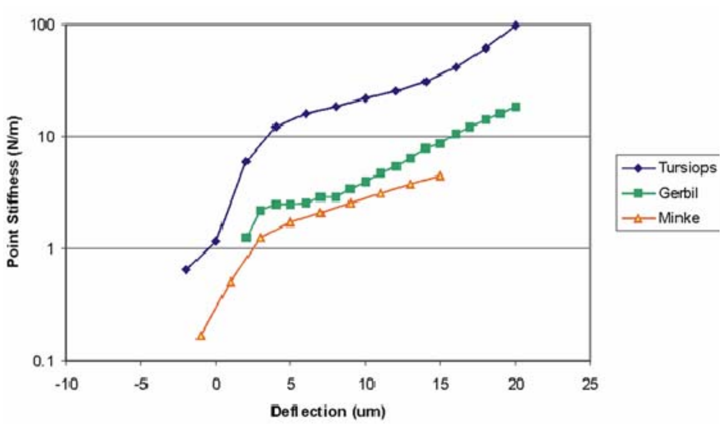

Figure 4. Comparison of the basilar membrane point stiffness measured in the base of the cochlea for three different species. The Minke result is significantly less stiff than that for Tursiopes and somewhat less stiff than found for gerbil.

It was not possible to get enough minke ears in good condition to estimate how stiffness changes with cochlear location so, for now, we are assuming that the minke stiffness gradient is similar to that in other mammals. Our basal turn stiffness data correspond to a predicted high-frequency limit for the Mike audiogram around 30 kHz.

Task 5: Simulation Studies

The anatomical reconstructions and estimated material properties were used to create a finite-element-method (FEM) model of the minke middle ear. The model was then used to predict the middle-ear transfer function by assuming that the acoustic input acts on the middle ear via the tympanic ligament. Figure 5 illustrates the FEM model.

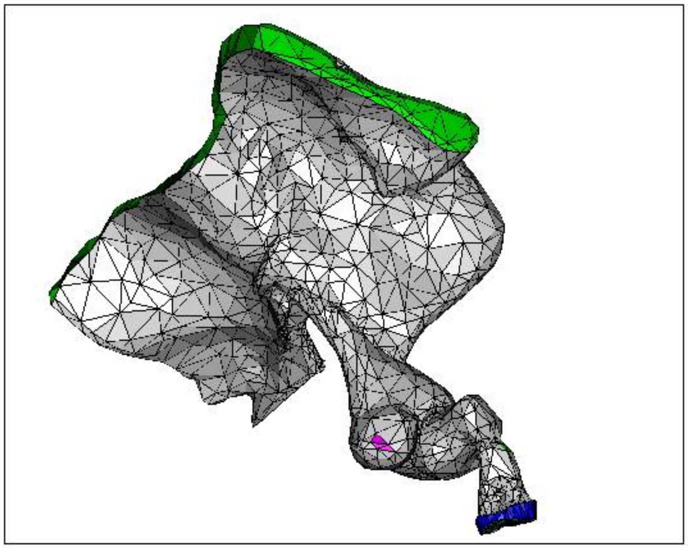

Figure 5. Minke middle-ear FEM model. The full model constains over 13,000 elements.

Figure 6 shows the predicted transfer function which was defined as the ratio of the stapes velocity to the input pressure. The most sensitive region is 100 Hz to 10 kHz. This transfer function was computed without cochlear loading. It is expected that with realistic cochlear loading that there will be some decrease in sensitivity at the lowest frequencies.

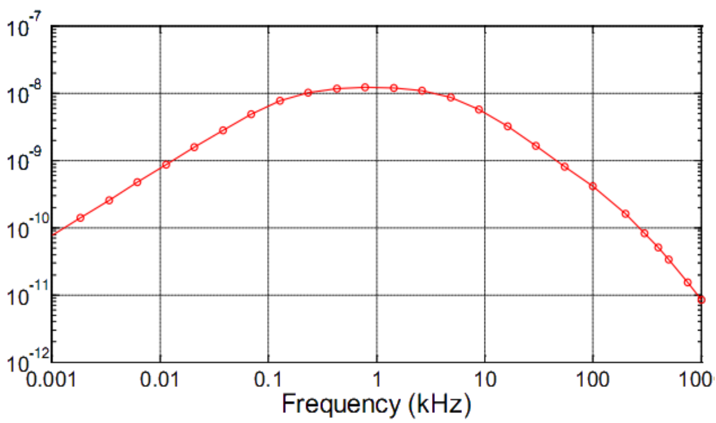

Figure 6. Predicted minke middle-ear transfer function.

For the cochlear modeling, three-dimensional reconstructions derived from CT scans were used to estimate the dimensions of the fluid compartments and the basilar membrane. The cross sectional areas of the fluid compartments were then used to compute the acoustic impedance of these compartments. These values along with the acoustic impedance estimates for the basilar membrane were then incorporated into a finite difference model This model is then used to estimate the cochlear input impedance which is the load seen by the middle ear at the stapes. To create an estimate of the minke audiogram we make the following assumptions.

- The middle-ear transfer function dominates the sensitivity in the low and mid-frequency regions.
- The sensitivity in the best frequency region is similar to that measured behaviorally in odontocetes

- The high frequency limit depends on the cochlear frequency-place map which can be derived from the basilar membrane stiffness map.

Figure 7 shows the resulting prediction for the audiogram. It is interesting to note that Gedamke, et al. (2001) reported that the minke vocal repertoire includes an unusual wide-band vocalization that has been called the "star-wars" vocalization. The frequency range (50 Hz – 9.4 kHz) of this vocalization lines up well with the sensitive region of the predicted audiogram. The predicted high-frequency limit of the audiogram (30 kHz) reaches into the range of the maximum energy (20-40 kHz) in the killer whale (Orcinus orca) echolocations signal (Au et al., 2004).

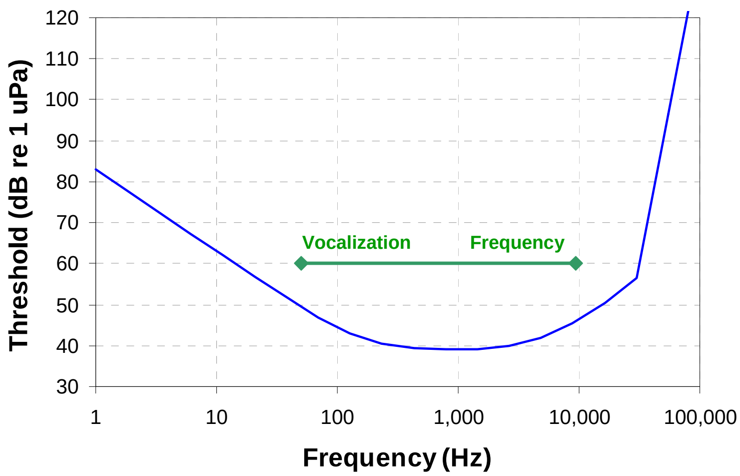

Figure 7. Preliminary prediction for the minke audiogram. The green bar shows the approximate frequency range for the "star-wars" vocalization.

Summary

We have refined our measurement and modeling techniques to the point where we have been able to produce a preliminary prediction for the minke audiogram. The predicted most sensitive region spans 40 Hz to 15 kHz which lines up well with the frequency range of vocalization in this species (50 Hz to 9.4 kHz).

AIM III

REPORTING/ EDUCATION/OUTREACH

Task 6: Reporting

This task comprised peer reviewed publication and development of website incorporating images and data from this project.

Milestones

6.1 Manuscript preparation and submission:

Publications related to this effort from are listed at the end of this report

6.2 Complete website development for WHOI scanner

The WHOI scanner website has been completed: http://csi.whoi.edu

Visualizations available include 2D series, 3D shaded surface reconstructions, and 3D multi-tissue reconstructions. Both still and animated data sets are represented for multiple species.

6.3 **Augment Boston University EarLab site with baleen data**

Website updates were completed.

Literature Cited

Au, WWL, Ford, JKB, and Home, JK (2004). Echolocation signals of free-ranging killer whales (Orcinus orca) and modeling of foraging for chinook salmon (Oncorhynchus tshawytscha). J. Acoust. Soc. Am. 115: 901-909.

Funnell, WRJ, Khanna, SM, Decraemer, WF. (1992) On the degree of rigidity of the manubrium in a finite-element model of the cat eardrum. J. Acoust. Soc. Am. 91: 2082-2090.

Ketten, D.R. (1994) Functional Analyses of Whale Ears: Adaptations for Underwater Hearing, *I.E.E.E Underwater Acoustics*, vol. 1, pp. 264 - 270.

Ketten. D.R. (1992) The Marine mammal ear: Specializations for aquatic audition and echolocation. In: *The Evolutionary Biology of Hearing*, D. Webster, R. Fay, and A. Popper (eds.), Springer-Verlag, pp. 717-750.

Ketten, D.R., Skinner, M., Wang, G., Vannier, M., Gates, and Neely, G. (1998) *In vivo* Measures of Cochlear Length and Insertion Depths of Nucleus® Cochlear Implant Electrode Arrays. *Annals of Otology and Laryngology*, vol. 107, no. 11, pp. 1-16.

Koopman, H.N., S.M. Budge, D.R. Ketten, and S.J. Iverson. (2006) The topographical distribution of lipids inside the mandibular fat bodies of odontocetes: Remarkable complexity and consistency. *IEEE Journal of Oceanic Engineering*, vol. 31(1), pp. 95-106.

Manoussaki, D., Chadwick, R.S, **Ketten**, D.R., Arruda, J., Dimitriadis, D., O'Malley, J.T. (2008)The Influence of Cochlear Shape on Low-Frequency Hearing. Proc. Natl. Acad. Sci, vol. 105(6): 6162-6166. (Featured Article of Issue)

Miller, B.S., Zosuls, A.L., Ketten, D.R. and Mountain, D.C. (2006). Middle ear stiffness of the bottlenose dolphin *Tursiops truncates*. IEEE J. Oceanic Eng. 31:87-94.

Mountain, D.C., Hubbard, A.E., Ketten, D.R. and O'Malley, J. (2003) The helicotrema: Measurements and models In: Biophysics of the Cochlea: from Molecule to Model. A.W. Gummer, E. Dalhoff, M. Nowotny, M. Scherer (Eds.). World Scientific, Singapore, pp.393-399.

Naidu, R.C. and Mountain, D.C. (1998). Measurements of the stiffness map challenge a basic tenet of cochlear theories. Hear. Res. 124: 124-131.

Olson, E. S. and Mountain, D. C. (1994) Mapping the cochlear partition's stiffness to its cellular architecture. J. Acoust. Soc. Am. 95: 395-400.

Predergast, PJ, Ferris, P, Rice, HJ, Blayney, AW. (1999) Vibro-acoustic modeling of the outer and middle ear using the finite element method. Audiol. Neurootol. 4: 185-191.

Rosowski JJ (1994) "Outer and Middle Ears," in Comparative Hearing: Mammals, R. R. Fay and A. N. Popper, Eds. New York: Springer-Verlag.

Sun, Q, Gan, RZ, Chang, K-H, Dormer, KJ. (2002) Computer-integrated finite element modeling of human middle ear. Biomech. Model Mechanobiol. 1: 109-122.

Project Related Publications

Publications

2008 Ketten, D.R. Underwater Ears and the Physiology of Impacts: Comparative Liability for Hearing Loss in Sea Turtles, Birds, and Mammals, *Bioacoustics, 17:*312-315.

2008 Yamato, M., Ketten, D.R., Arruda, J. & Cramer, S., 2008, Biomechanical and structural modeling of hearing in baleen whales. *Bioacoustics;* 17: 100-102.

2008 Manoussaki, D., Chadwick, R.S, Ketten, D.R., Arruda, J., Dimitriadis, D., O'Malley, J.T. The Influence of Cochlear Shape on Low-Frequency Hearing. *Proc. Natl. Acad. Sci*., vol. 105, no. 16: 6162-6166.

2008 Mountain, D.C., Zosuls, Z., Newburg, S., and Ketten, D.R.. Predicting cetacean audiograms. *Bioacoustics*, 17:77-80.

2008 Manoussaki, D., Chadwick, R.S, Ketten, D.R., Arruda, J., Dimitriadis, D., O'Malley, J.T. The Influence of Cochlear Shape on Low-Frequency Hearing. Proc. Natl. Acad. Sci, vol. 105(6): 6162-6166. (Featured Article of Issue)

2008 Ketten, D.R. Underwater ears and the physiology of impacts: Comparative liability for hearing loss in sea turtles, birds, and mammals. Bioacoustics, vol. 17, no. 1-3, pp. 312-315.

2010 Ketten, D.R. Marine Mammal Auditory System Noise Impacts: Evidence and Incidence. In: Proceedings of the Second International Conference on the Effects of Noise on Aquatic Life, A. Popper and T. Hawkins (eds). Springer-Verlag (accepted, in press).

Published Abstracts

2007 Ketten, D.R. Current Models of Baleen and Odontocete Whale Hearing: Evidence for Differences in Noise Impacts. NATO Intergovernmental Conference on The Effects of Sound in the Ocean on Marine Mammals, Lerici, Italy.

2007 Yamato, M., Ketten, D.R., Arruda, J., Cramer, S., Anatomical Studies of Mysticete Hearing: A Key to Understanding How and What Whales Hear. ASLO

2007 Yamato, M., Ketten, D.R., Arruda, J., and Cramer, S. Biomechanical and structural modeling of hearing in baleen whales. *Poster,* 15th Annual Southeast and Mid-Atlantic Marine Mammal Symposium (SEAMAMMS), Beaufort, NC. *Best Poster Award*.

2007 Yamato, M., D. R. Ketten, J. Arruda, and S. Cramer. Biomechanical and Structural Modeling of Hearing in Baleen Whales. 17th Biennial Conference on the Biology of Marine Mammals. Cape Town, South Africa.

2007 Ketten, D. R., Arruda, J, Cramer, S, Yamato, M., Zosuls, A.., Mountain, D. Chadwick, R. S., Dimitriadis, E. K., Shoshani, J., O'Connell-Rodwell, C. How Low Can They Go: Functional

analyses of the largest land and marine mammal ears. 17th Biennial Conference on the Biology of Marine Mammals. Cape Town, South Africa.

2007 Mountain, D.A, Zosuls, A.L., Newburg, S. O.,and Ketten, D.R. Predicting Cetacean Audiograms. . The Effects of Noise on Aquatic Life, Nyborg, Denmark.

2007 Yamato, M., Ketten, D.R., Arruda, J. & Cramer, S. Biomechanical and structural modeling of hearing in baleen whales. International Conference on The Effects of Noise on Aquatic Life, Nyborg, Denmark.

2007 Ketten, D.R. Underwater Ears and the Physiology of Impacts: Comparative Liability for Hearing Loss in Sea Turtles, Birds, and Mammals, *Invited plenary paper* The Effects of Noise on Aquatic Life, Nyborg, Denmark

2008 Mountain, D.C., Khan, A., Newburg, S., and Zosuls, A., and Ketten, D.R. The Biophysics of Cetacean Hearing. Second International Conference on Acoustic Communication by Animals, Corvallis, Oregon

2008 Mountain, D., Zosuls, A., Newburg, S, and Ketten, D. (2008) Cetacean Middle Ear and Basilar Membrane Mechanics. Association for Research in Otolaryngology

2009 Ketten, D.R. Underwater Ears and Potential Impacts: What whales can and cannot hear. Israeli Zoological Society, Keynote Lecture, University of Tel Aviv, Tel Aviv, Israel.

2009 Ketten, D. R., Yamato, M., Clark, C., Ellison, W., Mountain, D., Zosuls, A. Mysticete Hearing: Basso, Biosonar, or Both? Invited paper 5th Animal Sonar Symposium, Kyoto, Japan.

2010 Ketten, D.R. Marine Mammal Auditory System Noise Impacts: Evidence and Incidence. 2nd International Meeting on the Effects of Noise on Aquatic Life. Cork, Ireland.

2009 Tubelli, A., Zosuls, A., Ketten, D. and Mountain, D.C. (2009). A Finite Element Model of the Cetcean Middle Ear. Proceedings of the Society for Marine Mammalogy.18th Biennial Conference.

2009 Zosuls, A., Newburg, S.O., Tubelli, A.A., Mountain, D.C. and Ketten, D.R. (2009). Measurements of Mechanical Properties of Cetacean Ears.. Proceedings of the Society for Marine Mammalogy.18th Biennial Conference.

2009 Tubelli, A., Zosuls, A. and Mountain, D.C. (2009). Finite Element Modeling to Determine Cetacean Middle Ear Function. Assoc. Res. Otolaryngol. Abs. 33: 29

2010 Tubelli, A., A. Zosuls, D. R. Ketten and D. C. Mountain. Prediction of a Mysticete Audiogram via Finite Element Analysis of the Middle Ear. 2nd International Conference of the Effects of Noise on Aquatic Life, Cork, Ireland

2010 Zosuls, A., S. O. Newburg, D. R. Ketten and D. C. Mountain. Reverse Engineering the Cetacean Ear to Extract Audiograms. 2nd International Conference of the Effects of Noise on Aquatic Life, Cork, Ireland.

APPENDIX I – SPECIMEN ACQUISTION AND DISTRIBUTIONS

Minke Whale Tissues Collected and Retained by Ketten Laboratory from January 1, 2007 to Present:

Ketten Id	Scientific Name	Common Name	Specimen Source	Date Received	Sex	Tissue(s)	CT
B-acu21	*Balaenoptera acutorostrata*	Minke Whale	Joy Reidenberg	7/28/2008	M	Skull Ear (Rt) In-situ Ear (Lt) (Tymp. / Perio. Bones Sep.)	Yes
B-acu19	*Balaenoptera acutorostrata*	Minke Whale	Michael Moore	6/16/2008	F	Head (flensed & decerebrate) Larynx (piece) Ear (Rt) (intact) Eye (Rt) Histology Samples Ear (Lt) (intact)	Yes
B-acu18	*Balaenoptera acutorostrata*	Minke Whale	CCSN	8/6/2007	F	Head section (Lt) (Frozen) Jaw tissue (Rt) (10% Formalin) Brain (hemisected) (10% Formalin) Ear (Rt) (To David Mountain) Jaw Fats (Rt) (Frozen) Ear (Lt) (In-situ) (Frozen)	Yes
B-acu17	*Balaenoptera acutorostrata*	Minke Whale	Joy Reidenberg	7/25/2007	-	Ear (Rt) (Intact) (10% Formalin) Ear (Lt) (Intact) (Frozen) (To David Mountain)	Yes

Whole Heads Dissected	2
Skulls	1
Tympanic Bones (In-situ and Extracted)	8
Periotic Bones (In-situ and Extracted)	8

Minke Whale Tissues Collected and Retained Prior to January 1, 2007:

Ketten Id	Scientific Name	Common Name	Specimen Source	Date Received	Sex	Tissue(s)	CT
B-acu15	*Balaenoptera acutorostrata*	Minke Whale	Katie Touhey	7/2/2006	M	Head (Partially Flensed) (Frozen) Ear (Lt) (Tymp./Perio. Bones Sep.) (10% Formalin) Jaw Fats (Lt) (10% Formalin) Ear (Rt) (In-situ) (Frozen)	Yes
B-acu13	*Balaenoptera acutorostrata*	Minke Whale	Katie Touhey	6/17/2005	M	Head (Flensed) (Frozen) Mandible (Frozen) Ear (Lt) (Tymp./Perio. Bones Sep.) (10% Formalin) Ear (Rt) (Intact) (10% Formalin) Histo Samples (Sent to AFIP) Eyes (Rt & Lt) (10% Formalin) EAC (Rt & Lt) (10% Formalin)	Yes
B-acu12	*Balaenoptera acutorostrata*	Minke Whale	Roger Williams	6/2/2003	F	Ear (Lt) (Tymp./Perio. Bones Sep.) (10% Formalin) Flensed Skull (Frozen) EAC (Rt) (Frozen) Fat Samples (10% Formalin) Ear (Rt) (Tymp./Perio. Bones Sep.) (10% Formalin) Basal Hyoid (10% Formalin) Histology Samples (10% Formalin) Nasal Cavity (10% Formalin)	Yes
B-acu10	*Balaenoptera acutorostrata*	Minke Whale	Greg Early	11/10/1997	F	EAM (10% Formalin)	No
B-acu07	*Balaenoptera acutorostrata*	Minke Whale	Michael Moore	7/23/1997	M	Ears (Rt & Lt) (Intact) (Frozen)	No
B-acu06	*Balaenoptera acutorostrata*	Minke Whale	Greg Early	6/15/1997	F	Head Sections (Frozen) Peribullar Plexis (Ears) (Rt) & (Lt) (10% Formalin) Brain (10% Formalin) Larynx (Frozen)	Yes
B-acu03_04_05_11	*Balaenoptera acutorostrata*	Minke Whale	Greg Early	9/30/1996	-	Eye (Rt) (10% Formalin) Periotic Bone (Rt) (MS Slides) Periotic Bone (Lt) (Celloidin)	Yes

						Skull (Flensed and Dried On Display) EAC (10% Formalin) EAM (10% Formalin) Tympanic Bone (Rt) (10% Formalin) Tympanic Bone (Lt) (10% Formalin)	
B-acu01_02	*Balaenoptera acutorostrata*	Minke Whale	Michael Moore	8/7/1996	-	Tympanic Bone (Lt) (10% Formalin) Tympanic Bone (Rt) (10% Formalin)	No

Whole Heads Dissected	5
Tympanic Bones (In-situ and Extracted)	14
Periotic Bones (In-situ and Extracted)	12

Srandings Attended, Necropsies, Dissections, and a Summary of Findings to Date:

Date: **June 17, 2008**

Description: Minke Whale Stranding (single whale) (B-acu19)

Stranding Location: Nauset Beach, Orleans, Mass.

Necropsy Location: Marine Research Facility – Woods Hole Oceanographic Institution.

Condition: A floating carcass discovered June 14, 2008 with the liver and both kidneys missing although remaining viscera were intact (code 2). Additionally, the whale had scavenger damage along the torso and peduncle (shark bites). The head was received June 15, 2008, chilled, and dissected June 17, 2008.

Tissues Collected: Whole Head

Tissue Status: Dissected head tissues were frozen or chemically preserved and stored at the MRF Facility for future analysis.

Summary Findings: Evidence of prior entanglement (line impressions and lacerations around the rostrum / maxilla), and wet, bloodfilled lungs indicating the animal likely drowned. Both lungs were wet and dark maroon (internally); the bronchial mucosa was dark red. No froth was present in lungs, but dark red fluid exuded when squeezed. After CT scanning the whole head, right ear was extracted. The body of fat similar to acoustic fats and associated with the tympanic membrane was reconfirmed. The extracted right ear was CT scanned and preserved in formalin. To reduce artifacts, a block of tissue surrounding the left ear was removed from the rest of the head and CT scanned. The superior image quality allowed for more accurate 3D reconstructions and volume estimates. MRI was also completed on this block of tissue

---

Date:	**August 8, 2007**
Description:	Minke Whale Stranding (single whale) (B-acu18)
Stranding Location:	Cornhill Beach, Truro, Mass.
Necropsy Location:	Marine Research Facility – Woods Hole Oceanographic Institution.
Condition:	A floating carcass discovered entangled in fishing gear considered moderately decomposed (code 3).
Tissues Collected:	Whole Head
Tissue Status:	Dissected head tissues were frozen or chemically preserved and stored at the MRF Facility for future analysis. The right ear with surrounding tissues was sent to the David Mountain Laboratory for analysis.
Summary Findings:	Chronic entanglement with severe emaciation resulting in dehydration and loss of protein; severe edema and septicemia of multiple tissues. Right ear was extracted. Findings included a body of fat similar to the acoustic fats of odontocetes, located in the ear region. This fat was extracted and frozen for future analyses. The left ear was kept intact and was CT scanned with the rest of the head, which was then stored in the freezer. Extracted right ear was CT scanned and taken to Boston University for further examination.

Minke Specimens scanned 2007-2008

B-acu15

12-Mar-08 / Frozen head rescanned for National Geographic demonstration-comparison of mysticete ears

B-acu17

17-May-07 / Right and Left ears received from Joy Reidenberg. Both ears scanned

at 3mm slice thickness resolution through entire ear blocks. Each ear then rescanned at 0.5mm slice thickness with 0.1mm reconstructions through periotic/tympanic regions.

2D soft tissue/bone window & 3D reconstruction formats.

28-Sep-07 / Left ear brought to MEEI for MRI scanning. Frozen, limited study

15-Feb-08 / Left ear brought to MEEI for MRI scanning. Better resolution. T1 & T2 high resolution imaged obtained.

B-acu18

6-Aug-07 / Head and ears scanned at 3mm slice thickness through head and 0.5mm slice thickness through ears. (S. Cramer scanned specimen) 2D soft tissue/bone window & 3D reconstruction formats. Filmed.

7-Aug-07 / Right extracted ear scanned using 2 spiral scans at 0.5mm thickness through entire ear with 0.1mm reconstructions through cochlea. 2D soft tissue/bone window & 3D reconstruction formats. (S. Cramer scanned specimen)

B-acu19

18-Jun-08 / Head and ears scanned at 3mm slice thickness through head using 2 spiral scans, and 1mm slice thickness through ears. 2D soft tissue/bone window & 3D reconstruction formats. Filmed.

24-Jun-08 / Rescanned upper head with lower jaw removed, still had penetration artifacts, removed additional skull base bone and scanned again at 1mm slice thickness through fats and left ear.

3-Jul-08 / Right extracted ear scanned using 3 spiral scans at 0.5mm thickness through entire ear with 0.1mm reconstructions through entire ear. 2D soft tissue/bone window & 3D reconstruction formats.

18-Jul-08 / Left ear block with fats scanned to obtain parameters for trimming and thawing prior to MRI scanning. (DRK scanned specimen)

21-Jul-08 / Left ear block with fats brought to MEEI for MRI scanning. High resolution T2 images obtained.

6-Aug-08 / Left ear block rescanned to correlate with MRI image positions.

B-acu20

29-Jul-08 / Flensed minke skull received from Joy Reidenberg. Scanned entire skull at 3mm slice thickness using 2 spiral scans, and 1 spiral at 0.5mm slice thickness. 2D bone window & 3D reconstruction formats.

B-acu21

6-Aug-08 / Right tympanic bone from another larger skull received from Joy Reidenberg. Skull too large to fit through gantry. 0.5mm slice thickness, which included separated malleus. 2D bone window & 3D reconstruction formats.

All specimens have images archived to CD and raw data archived to MOD.

Head and Ear Morphometry

B-acu11 Measurements on skull:

Width of skull between anterior prominence of squamosal bones:41.5cm

Width of skull between posterior prominence of parietal bones: 40.0cm

Length of skull from occipitals to rostrum: at least 85.5cm

Distance through right and left occipital bones at ventral margin of foramen magnum: 12.6cm

B-acu13 3D reconstructions of the head and left ear region, including fats.

Approximate volume of fats around the left ear: 767cm^3 (3.89m animal)

*There is too much artifact in the CT images to get accurate volume

B-acu15 3D reconstructions of the head and right ear region, including fats.

Approximate volume of fats around the right ear: 1580cm^3 (4.6m animal)

B-acu17 3D reconstructions of the left ear, including the cochlea, glove finger, and ossicles.

Measurements on skull (bone around ears has been removed):

Width of skull between posterior prominence of parietal bones: 48.7cm
Length of skull from occipitals to rostrum: at least 94cm
Length of right mandible: 92.3cm
Coronoid process to posterior end of right mandible: 18.2cm
Length of left mandible: 92.2cm
Coronoid process to posterior end of left mandible: 18.5cm

B-acu19 3D reconstructions of the head and left ear region, including fats.
Approximate volume of fats around left ear: 1387cm^3 (4.26m animal)

B-acu20 Measurements on skull:
Width of skull between anterior prominence of squamosal bones: 53.3cm
Width of skull between posterior prominence of parietal bones: 52.2cm
Length of skull from occipitals to rostrum: 111.7cm
Distance through right and left occipital bones at ventral margin of foramen magnum: 13.6cm
Horizontal diameter of foramen magnum: 6.6cm at posterior, outer edge; 5.8cm at anterior, inner edge
Vertical diameter of foramen magnum: 4.6cm
Distance between lateral processes of right and left tympanic bones: 22.1cm
Length of right tympanic bone from the sharp edge at anterior margin to the posterior sharp edge: 8.0cm
Length of left tympanic bone from the sharp edge at anterior margin to the posterior sharp edge: 8.0cm

B-acu21 Measurements on skull:
Width of skull between anterior prominence of squamosal bones: 71.0cm
Width of skull between posterior prominence of parietal bones: 69.4cm
Length of skull from occipitals to rostrum: 136.3cm
Distance through right and left occipital bones at ventral margin of foramen magnum: 17.1cm
Horizontal diameter of foramen magnum: 7.5cm at posterior, outer edge; 6.3cm at anterior, inner edge

Vertical diameter of foramen magnum: 5.5cm

Distance between lateral processes of right and left tympanic bones: 27.6cm

Length of right tympanic bone from the sharp edge at anterior margin to the posterior sharp edge: 8.4cm

Length of left tympanic bone from the sharp edge at anterior margin to the posterior sharp edge: 8.4cm

SPECIMENS FOR HISTOLOGY

B-acu04	Left periotic bone in celloidin block
B-acu07	Left and right ears frozen
B-acu12	Left and right ears fixed in formalin
B-acu13	Left and right ears fixed in formalin
B-acu15	Left ear in fixed in formalin, right ear in frozen head
B-acu17	Right ear fixed in formalin
B-acu18	Right ear in David Mountain’s lab, left ear in frozen head
B-acu19	Right ear fixed in formalin, left ear in frozen head